A Power Control Scheme for the Islanding Transition of a Microgrid with Battery Energy Storage Systems

Juan Diego Rios Penaloza
Department of Electrical, Electronic and Information Engineering
University of Bologna
Italy
juan.riospenaloza3@unibo.it

James Amankwah Adu
Department of Electrical, Electronic and Information Engineering
University of Bologna
Italy
jamesamankwah.adu@unibo.it

Alberto Borghetti
Department of Electrical, Electronic and Information Engineering
University of Bologna
Italy
alberto.borghetti@unibo.it

Fabio Napolitano
Department of Electrical, Electronic and Information Engineering
University of Bologna
Italy
fabio.napolitano@unibo.it

Fabio Tossani
Department of Electrical, Electronic and Information Engineering
University of Bologna
Italy
fabio.tossani@unibo.it

Carlo Alberto Nucci
Department of Electrical, Electronic and Information Engineering
University of Bologna
Italy
carloalberto.nucci@unibo.it

***Abstract*—This paper focuses on the analysis of the dynamic behavior of an AC microgrid including rotating and stationary loads and battery energy storage systems during unplanned islanding transitions. The signal necessary to switch from grid-connected to standalone control mode is not instantaneous. The delay might be so long to result in frequency and voltage transients that could lead to the instability of the microgrid. The aim of this paper is to assess the potential benefits resulting from the implementation of an active and reactive power control scheme able to allow, starting from a grid-connected operation, a successful transition to island. The influence of different percentages of rotating load connected to the microgrid is analyzed by using EMTP-RV and time domain simulations of a modified version of the IEEE 34-bus test distribution system in which two battery energy storage systems are connected to two different buses.**

Keywords—Battery energy storage system, Distributed energy resource, Frequency control, Islanding, Microgrid, Power converter, EMTP.

I. INTRODUCTION

The progressively increasing connection of Distributed Energy Resources (DER) to the distribution network makes it worth of investigation the potential exploitation of Microgrids (MG) to increase the reliability of power supply.

For such a purpose, DERs connected to the network through power converters (e.g., photovoltaic systems, wind turbines, batteries and fuel cells) can operate in both grid-connected and standalone control modes. Indeed, on an islanding transition, inverter-interfaced DERs need to switch from grid-connected to standalone control mode in order to guarantee both frequency and voltage stability of the MG. The switch can be triggered by different islanding detection methods [1], which can be classified as local methods, based on measurements at the MG side (as in [2]), and remote methods, based on signals sent by the circuit breaker relay at the point of common coupling (PCC) (as in [3], [4]) or by a central controller (as in [5]–[8]).

When islanding occurs, the frequency deviation can be very fast if the MG is fed only by inverter-interfaced DERs, due to the absence of inertia [9]. The change of the power electronic converter control mode is not instantaneous but depends on the islanding detection strategy. According to the results reported in [10], the detection phase could take up to a few hundreds of milliseconds, if a local islanding detection method is employed, and several tens of milliseconds, if a signal is sent to the inverter. For long delays, the frequency and voltage transients could lead to the instability of the microgrid. For example, in [5] it has been shown that an experimental inertia-less system can avoid instability only for switching delays shorter than 470 ms.

This paper focuses on a control strategy of power converters aimed at reducing the frequency and voltage deviations of the MG during the power converter change of operation mode, in order to improve the power supply continuity also in case of unplanned islanding transitions.

In the literature on the subject, a few studies explicitly consider the delay in the control model change (e.g. [5], [8], [11]), whilst most studies consider that such switch happens simultaneously to the island formation (e.g. [3], [4], [6], [7]).

Within this context, we analyze the advantages of an adaptive droop control in the grid-connected control mode in order to keep the frequency and voltage stability of a medium voltage MG within acceptable values although power converters continue to operate in grid-connected mode during unplanned islanding transitions. The aim of the proposed control is to provide synthetic inertia to the system.

In particular, the advantages of the proposed control scheme for different MG load composition (static and rotating loads) on the frequency response are assessed through the results of computer simulations for the case of a modified version of the IEEE 34-bus test system in which two battery energy storage (BES) systems are added. The simulations are carried out by using the Electromagnetic Transient Program (EMTP-RV).

The structure of the paper is the following. Section II briefly describes the typical inverter control strategy and the proposed control scheme of the power converter of a BES

The research activity is carried out in the framework of the PODCAST project (platform for the optimization of the distribution using data from smart meters and distributed storage systems), partially funded by MISE (Italian Ministry for Economic Development).

978-1-7281-0653-3/19/$31.00 ©2019 IEEE

system. Section III describes the model of the MG considered for the analysis and implemented in the EMTP-RV simulation environment. Section IV and V present the simulation results for the different control strategies and for different types of load composition, respectively. Section VI concludes the paper.

II. Inverter Control Strategies

It is assumed that the dynamic behavior of the considered MG is mainly governed by the control strategy of the BES power converters. The control strategies are different in grid-connected and standalone operation modes [12], as briefly described in the following.

In the grid-connected mode, active and reactive power outputs are controlled as shown in Fig. 1. In a typical strategy this is achieved by using the *dq*-frame [13] and the angle reference provided by a Phase-Locked Loop (PLL). The final control output $v_{abc,ref}$ is the reference to the PWM control of the power converter.

In the standalone mode voltage and frequency are controlled, while active and reactive power outputs are defined by the load demand, as shown in Fig. 2

A. Conventional droop control

As shown in Fig. 1, the conventional droop control modifies the power reference in order to respond accordingly to generation/load variations, by adding the following quantity,

$$P' = \frac{1}{k_P}\left(f_{ref} - f\right) \tag{1}$$

$$Q' = \frac{1}{k_Q}\left(v_{ref} - v\right) \tag{2}$$

thus,

$$P^* = P_{ref} + P' \tag{3}$$

$$Q^* = Q_{ref} + Q' \tag{4}$$

where f_{ref}, v_{ref}, P_{ref}, and Q_{ref} are the reference values for the frequency, voltage, active and reactive powers, respectively, k_P and k_Q are the droop constants for active and reactive power control, respectively and, P^* and Q^* are the reference values modified by the droop control.

The conventional droop control strategy is the one commonly applied for voltage and frequency control in power systems with predominantly reactive equivalent impedance and large inertia.

B. Proposed active power control

Conventional droop control might present, among other limitations, an unsatisfactory transient response [14], [15], therefore alternative control strategies are proposed in the literature (e.g., [16], [17]) to improve the system stability while ensuring power sharing in the standalone control mode.

This paper proposes the adoption of a power control scheme which dynamic response takes advantage of the presence of an input signal proportional to the rate of change

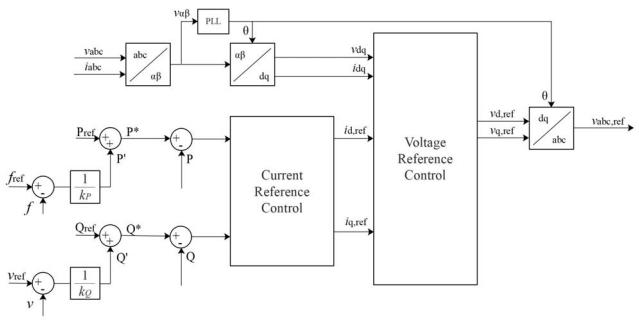

Fig. 1. Control scheme of the grid-connected mode with conventional droop characteristic. PLL is the phase-locked loop, PI a proportional integral controller, *αβ* and *dq* are the Clarke's and Park's transformations. The measured quantities are f, v_{abc}, i_{abc}, P, and Q .

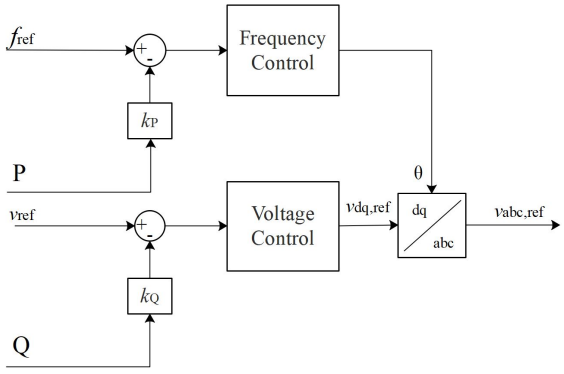

Fig. 2. Typical scheme of the standalone control mode with droop characteristics. The measured quantities are P and Q.

of frequency (ROCOF), analogously to typical speed governors with a tacho-accelerometer. In particular, the ROCOF (in s^{-1}) is calculated as in conventional relays [18],

$$ROCOF = \frac{1}{n} \times \sum_{i=1}^{n} \frac{\Delta f_i}{\Delta t_i} \tag{5}$$

$$\text{with} \qquad n = f_s \times \Delta t_w \tag{6}$$

where Δf_i is the p.u. frequency variation in the step time Δt_i, Δt_w is the time window in which measurements are taken, equal to 5 cycles of the power frequency and f_s is the sampling frequency (equal to 2 kHz in the analysis of this paper).

The ROCOF signal is implemented in the proposed control scheme as in Fig. 3, i.e. as an independent input signal that modifies the regulator gain model as follows,

$$P' = \frac{1}{k_{ROCOF}} \Delta f \tag{7}$$

$$k_{ROCOF} = \frac{k_P}{1 - k_f \times ROCOF \times \Delta f} \tag{8}$$

where k_f is a constant (in s) and Δf is the frequency error in p.u.

The reactive power is controlled by the conventional droop strategy of Fig. 1.

III. The Model of the Microgrid

Fig. 4 shows the scheme of the modified IEEE 34-bus test feeder considered for the analysis.

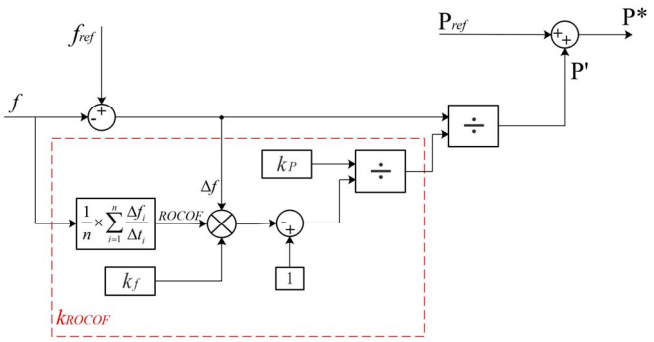

Fig. 3. ROCOF implemented in the adopted control strategy.

Each of the two BES units consists of a battery with 560 kWh capacity connected to the network through a 720-kVA power electronic converter. The adopted model for the battery is based on a Thévenin's equivalent circuit. The dynamic response is modelled by three RC branches in series with the battery resistance which values depend on the state of charge and are chosen as in [19]. The state of charge has been assumed to remain constant during the transients considered in this paper, as in [20]. The power converters are represented by the average model, which is suitable for determining the frequency transients of the network [21], [22].

The network model has been implemented in the EMTP-RV simulation environment. The MG under analysis is the portion disconnected from the rest of the network by the circuit breakers CB1 and CB2 open. The total load connected to the MG is 865 kW. The load is composed by both static and rotating components.

IV. Comparison Between Control Strategies

Three different initial steady state conditions are considered for the analysis:

1. Both BES units are supplying the same active power and the sum is lower than that required by the MG. The rotating load is 30% of the total.
2. Same as case 1, except for the rotating load that is 75% of the total.
3. Both BES units are suppling the same active power and the sum is larger than the power required by the MG, thus, before islanding, the MG is exporting active power to the main network. The rotating load is 30% of the total.

In the previous cases there is no switching to the standalone control mode. We consider also a fourth case, with the same steady state condition of case 1, in which the operating mode switching takes place 400 ms after the islanding transition.

The islanding process is simulated by opening circuit breakers CB1 and CB2 simultaneously at t=0 s. The values of the control parameters chosen for the simulation are reported in Table I. k_P is selected among typical values, k_Q is set to 10%, so that the BES unit supplies/absorbs all its reactive power in correspondence of a voltage deviation of ±0.1 p.u., while k_f is inferred through trial and error.

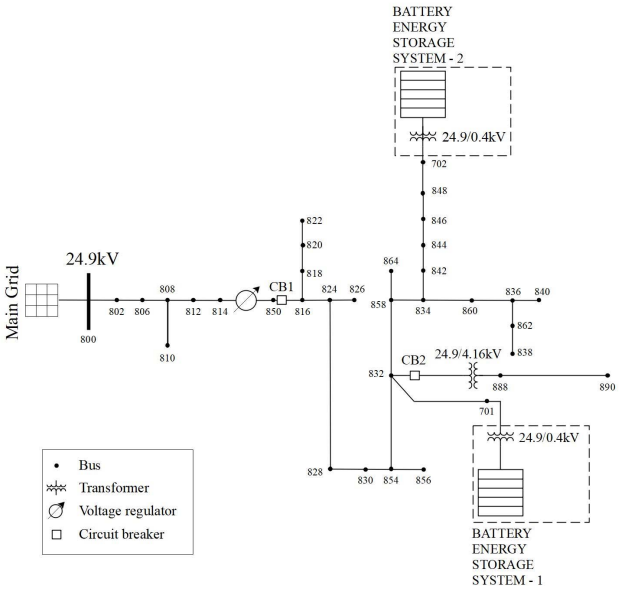

Fig. 4. Considered network: IEEE 34-bus test feeder with two BES systems. In the islanding, circuit breakers CB1 and CB2 open. Stationary and rotating loads are distributed at various nodes.

TABLE I. Control Parameters

Parameter	Value
k_P	$1\ \%$ or $4.36 \times 10^{-6}\ \frac{\text{rad/s}}{\text{W}}$
k_Q	$10\ \%$ or $3.458 \times 10^{-3}\ \frac{\text{V}}{\text{Var}}$
k_f	350 s

A. Case 1

Before islanding, both BES units are providing 0.1 p.u. of active power, thus injecting a total of 144 kW to the grid. When islanding occurs a negative power imbalance of 721 kW is produced. The rotating load is 30% of the total.

Fig. 5 shows the comparison between the frequency and voltage transients during the islanding transition with and without the adaptive droop control. The voltage is measured at bus 822 in Fig. 4, in which an asynchronous motor is connected. The proposed control strategy allows to keep frequency and voltage within acceptable limits, while the conventional droop control does not.

In Fig. 6 the transient of k_{ROCOF} is illustrated together with those of the system frequency and the ROCOF.

B. Case 2

Considering the same initial conditions for both BES units as for the previous case with 75% of rotating load connected to the MG, Fig. 7 shows the comparison of the frequency and voltage transients during the islanding transition. In this case, both frequency and voltage transients are not affected by the presence of the adaptive control.

As expected, the final frequency is the same for both strategies as the droop characteristics are the same in steady-state.

C. Case 3

Before islanding, both BES units are providing 1 p.u. of active power, thus feeding the network with 1440 kW. The MG is exporting 575 kW of active power to the main network. Fig. 8 shows the comparison of the frequency and voltage transients during the islanding transition with and without the adaptive droop control. The rotating load is 30% of the total.

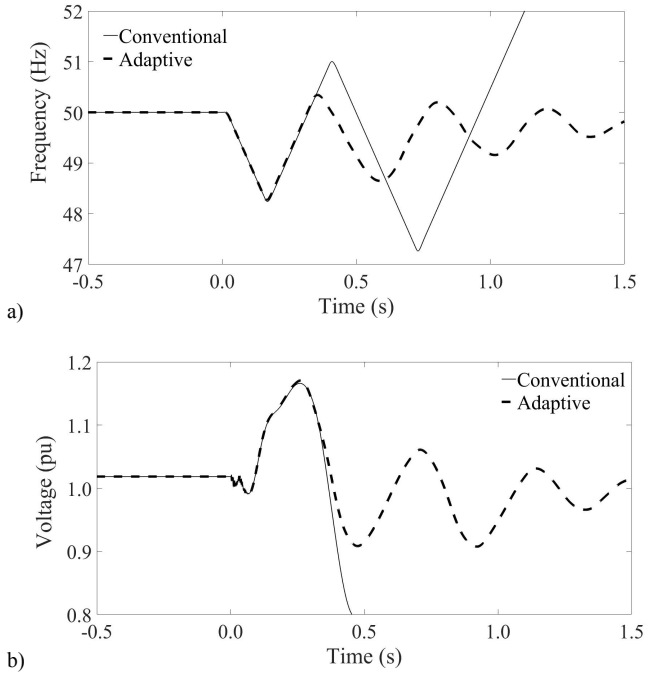

Fig. 5. Case 1: a) frequency and b) voltage transients during islanding for both, conventional and adaptive droop control.

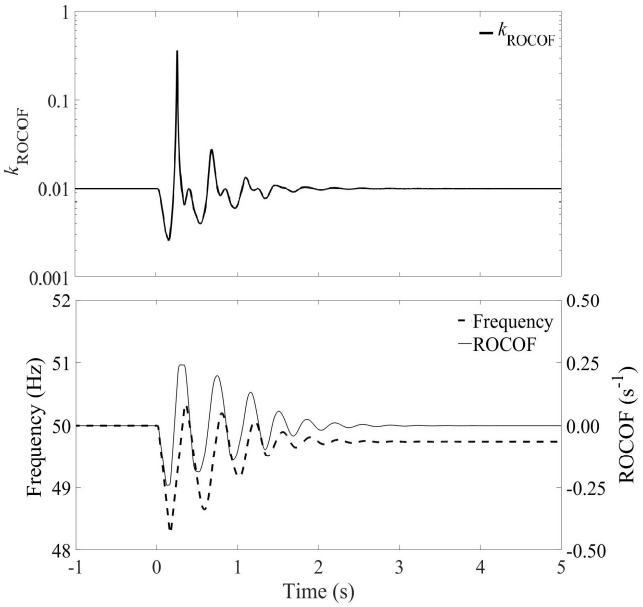

Fig. 6. Case 1: variation of k_{ROCOF}, frequency, and the ROCOF, during the islanding transition.

D. Case 4

The initial conditions before islanding are the same of case 1. Fig 9 shows the comparison of the frequency and voltage transients with and without the adaptive control, assuming that the switching signal arrives 400 ms after the opening of CB1 and CB2.

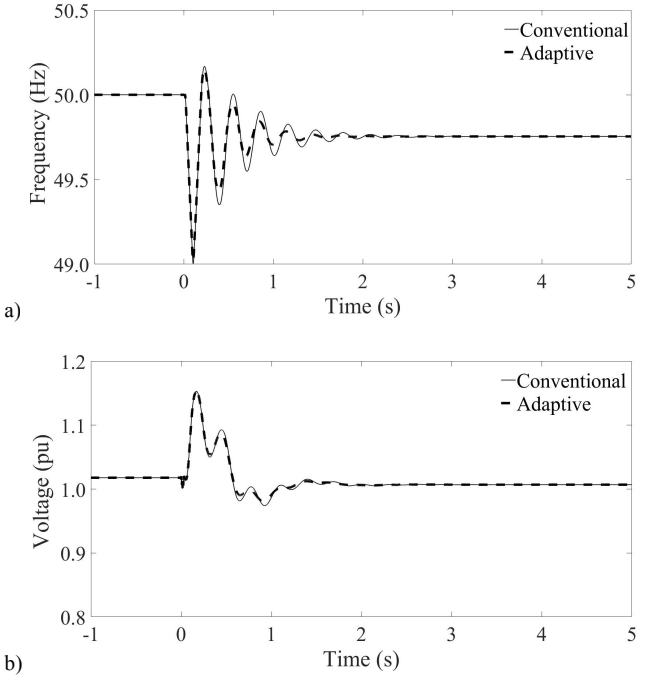

Fig. 7. Case 2: a) frequency and b) voltage transients during islanding for both, conventional and adaptive droop control.

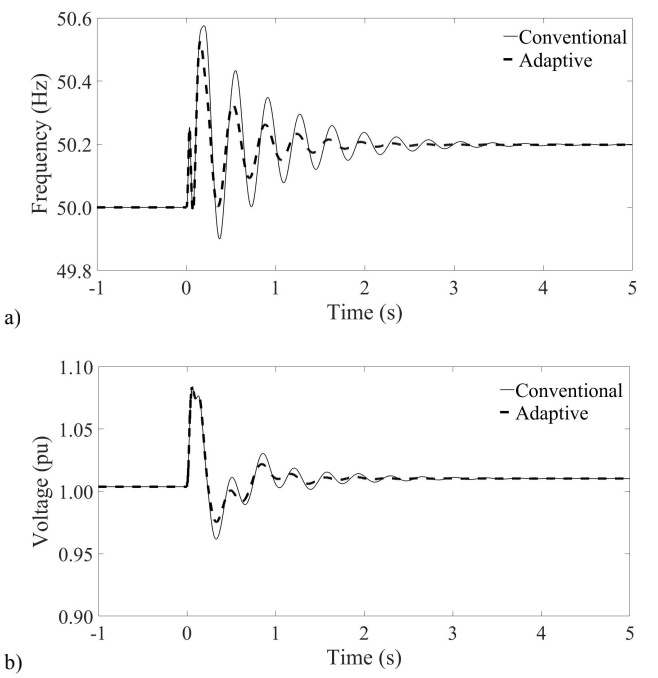

Fig. 8. Case 3: a) frequency and b) voltage transients during islanding for both, conventional and adaptive droop control.

V. Simulation Results for Different Load Composition

The inertia of rotating masses in a power system has a significant impact on the frequency transient. In the system under analysis, the inertia of the MG is given only by the rotating component of the load. In this section, we consider different percentages of rotating load connected to the MG and, for each load composition, the critical time delay for the switching from grid-connected to standalone mode is calculated.

As in the previous section, the islanding process is simulated by opening circuit breakers CB1 and CB2 simultaneously at t=0 s. Before islanding we assume that the system is in the same steady state conditions described by case 1.

Besides frequency instability, voltage drop might cause cascading events in the MG, as reported e.g. in [5]. For an estimation of the critical time delays for the switching signal, two criteria have been assumed for which the MG is declared unstable: i) frequency deviates over 52 Hz or under 47 Hz and; ii) voltage drop at any of the motor terminals exceeds 20% of its nominal value.

For different load composition, the critical time delays are reported in Table II. Apart from the first case, where is the frequency criterion i) that determines the maximum time delay, for all other cases it is determined according to voltage criterion ii). The rotating load percentage is increased by randomly adding asynchronous motors at different nodes of the network. The criterion of 20% voltage drop is therefore reached at different nodes at different times since the voltage variation is not the same for all buses. As a matter of fact, maximum time delay values do not necessarily increase linearly with the rotating load percentage, as it could be expected.

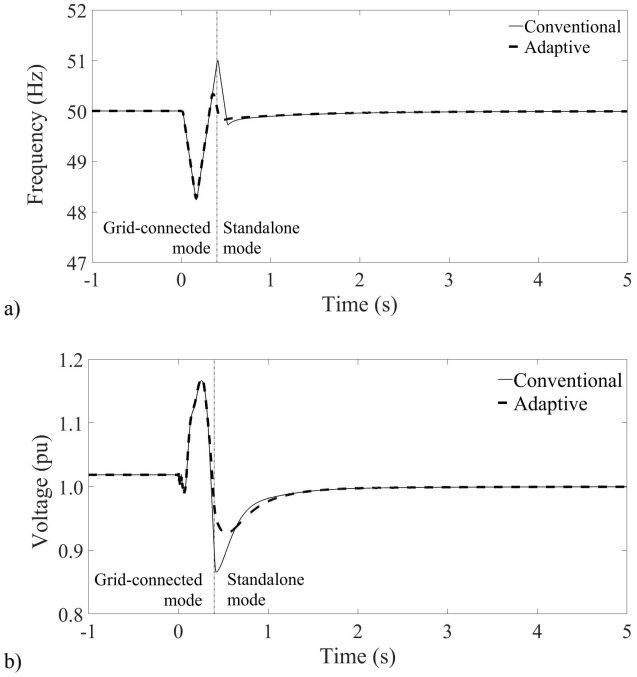

Fig. 9. Case 4: a) frequency and b) voltage transients during islanding for both, conventional and adaptive droop control.

For the cases in which system stability is guaranteed even if the switching signal does not arrive to the power converter (i.e. there is not a maximum time delay), for illustrative purposes Table II shows the frequency nadir and minimum voltage values instead of the maximum time delay. The possibility to limit the frequency and voltage deviations and to keep the continuity of the power supply in the studied MG is related to the ratio between static and rotating load components. For the considered test case, if the percentage of rotating load is large, namely more than 50% of the total load, the conventional droop frequency control maintains the stability during the islanding transition, regardless of the delay of the switching signal. Concerning the adaptive droop control, the delay of the islanding detection signal is no more critical for the vast majority of cases, except for the one in which the rotating load is 5% of the total.

Now we assume that, before islanding, the steady state condition of the MG is the one described as case 3. In such situation both the conventional and adaptive droop controls are able to maintain stability for all the simulation cases. In Fig. 10 the maximum values of frequency reached during the transient are reported. Results for both control methods are very similar.

TABLE II. Maximum switching time delays, frequency nadir and minimum voltage values, for different percentages of rotating load. The MG is importing active power before islanding.

Rotating load (%)	Conventional droop control			Adaptive droop control		
	Max. time delay (ms)	Freq. nadir (Hz)	Min. voltage (pu)	Max. time delay (ms)	Freq. nadir (Hz)	Min. voltage (pu)
5	268.0	--	--	268.0	--	--
10	663.0	--	--	--	47.172	0.889
15	509.0	--	--	--	47.577	0.857
20	455.0	--	--	--	47.851	0.855
25	427.0	--	--	--	48.091	0.881
30	432.0	--	--	--	48.270	0.908
35	800.0	--	--	--	48.442	0.899
40	753.5	--	--	--	48.590	0.907
45	749.0	--	--	--	48.690	0.921
50	--	48.762	0.896	--	48.789	0.934
55	--	48.828	0.925	--	48.850	0.946
60	--	48.883	0.942	--	48.903	0.957
65	--	48.929	0.957	--	48.947	0.969
70	--	48.970	0.968	--	48.987	0.979
75	--	49.003	0.974	--	49.019	0.981
80	--	49.036	0.975	--	49.051	0.981
85	--	49.066	0.977	--	49.081	0.982
90	--	49.094	0.978	--	49.107	0.983
95	--	49.122	0.979	--	49.135	0.984
100	--	49.139	0.982	--	49.151	0.986

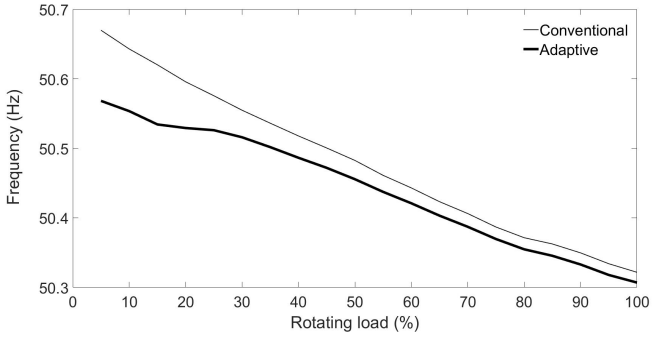

Fig. 10. Maximum frequency values reached during islanding transition for different percentages of rotating load. The MG is exporting active power to the main network before islanding.

VI. Conclusions

The frequency dynamic behavior of a MG including rotating and static loads and two BES units when unplanned islanding occurs has been analyzed with the aim to assess the benefits of an adaptive droop control of the two power converters interfacing the BES units to the MG.

We focused on the grid-connected control mode of the converter as, for the islanding transition of a MG, the signal necessary to switch from grid-connected to standalone control mode is not instantaneous. The switching delay might be so large to result in a fast and dangerous drop of the MG frequency and voltage. The proposed control scheme employs a rate of change of frequency signal, as such strategy is the one expected to improve the frequency and voltage transients.

By means of time domain simulations carried out by using an EMTP-RV model of a MG, it has been shown that, when islanding occurs, power converters controlled with the conventional droop strategy must switch from grid-connected to standalone mode within a short time in order to hold the system stability, particularly when the MG is importing active power from the main network before islanding. The maximum relevant times for such a change were estimated and the dependence on the amount of rotating load was illustrated. With the adaptive droop control that enhances the stability of the MG during islanding transition, the delay of the signal to change between control modes is not critical.

The EMTP-RV simulation results show that for large percentages of rotating load, namely more than 50% of the total load for the considered MG, the conventional droop control method can guarantee the continuity of the power supply during the islanding transition; however, for lower percentages of rotating load, only the proposed adaptive droop control succeeds in maintaining the stability of the system.

References

[1] C. Li, C. Cao, Y. Cao, Y. Kuang, L. Zeng, and B. Fang, "A review of islanding detection methods for microgrid," *Renew. Sustain. Energy Rev.*, vol. 35, pp. 211–220, 2014.

[2] I. J. Balaguer, Q. Lei, S. Yang, U. Supatti, and F. Z. Peng, "Control for Grid-Connected and Intentional Islanding Operations of Distributed Power Generation," *IEEE Trans. Ind. Electron.*, vol. 58, no. 1, pp. 147–157, 2011.

[3] R. Caldon, M. Coppo, A. Raciti, and R. Turri, "Dynamic control of inverter-connected generators for intentionally islanded MV distribution networks," in *Proceedings of the Universities Power Engineering Conference*, 2013.

[4] R. Caldon, A. Stocco, and R. Turri, "Feasibility of adaptive intentional islanding operation of electric utility systems with distributed generation," *Electr. Power Syst. Res.*, vol. 78, no. 2008, pp. 2017–2023, 2017.

[5] A. Cagnano, E. De Tuglie, and L. Cicognani, "Prince — Electrical Energy Systems Lab: A pilot project for smart microgrids," *Electr. Power Syst. Res.*, vol. 148, pp. 10–17, 2017.

[6] J. Kim, J. Jeon, S. Kim, C. Cho, J. H. Park, H. Kim, and K. Nam, "Cooperative Control Strategy of Energy Storage System and Microsources for Stabilizing the Microgrid during Islanded Operation," *IEEE Trans. Power Electron.*, vol. 25, no. 12, pp. 3037–3048, 2010.

[7] J. Wang, N. C. P. Chang, X. Feng, and A. Monti, "Design of a Generalized Control Algorithm for Parallel Inverters for Smooth Microgrid Transition Operation," *IEEE Trans. Ind. Electron.*, vol. 62, no. 8, pp. 4900–4914, 2015.

[8] A. Cagnano, E. De Tuglie, M. Trovato, L. Cicognani, and V. Vona, "A simple circuit model for the islanding transition of microgrids," in *IEEE 2nd International Forum on Research and Technologies for Society and Industry Leveraging a Better Tomorrow, RTSI*, 2016.

[9] N. Pogaku, M. Prodanović, and T. C. Green, "Modeling, analysis and testing of autonomous operation of an inverter-based microgrid," *IEEE Trans. Power Electron.*, vol. 22, no. 2, pp. 613–625, 2007.

[10] W. El-Khattam, T. S. Sidhu, and R. Seethapathy, "Evaluation of two anti-islanding schemes for a radial distribution system equipped with self-excited induction generator wind turbines," *IEEE Trans. Energy Convers.*, vol. 25, no. 1, pp. 107–117, 2010.

[11] F. Katiraei, M. R. Iravani, and P. W. Lehn, "Micro-Grid Autonomous Operation During and Subsequent to Islanding Process," *IEEE Trans. Power Deliv.*, vol. 20, no. 1, pp. 248–257, 2005.

[12] S. Barsali, M. Ceraolo, P. Pelacchi, and D. Poli, "Control techniques of Dispersed Generators to improve the continuity of electricity supply," in *IEEE Power Engineering Society Winter Meeting*, 2002, pp. 789–794.

[13] C. Schauder and H. Mehta, "Vector analysis and control of advanced static VAR compensators," *Proc. Inst. Elect. Eng., Gen.,Transm., Distrib.*, vol. 140, no. 4, pp. 299–306, 1993.

[14] E. Rokrok, M. Shafie-khah, and J. P. S. Catalão, "Review of primary voltage and frequency control methods for inverter-based islanded microgrids with distributed generation," *Renew. Sustain. Energy Rev.*, vol. 1, no. 82, pp. 3225–3235, 2018.

[15] J. C. Vasquez, R. A. Mastromauro, J. M. Guerrero, and M. Liserre, "Voltage support provided by a droop-controlled multifunctional inverter," *IEEE Trans. Ind. Electron.*, 2009.

[16] J. M. Guerrero, L. G. de Vicuna, J. Matas, M. Castilla, and J. Miret, "A wireless controller to enhance dynamic performance of parallel inverters in distributed generation systems," *IEEE Trans. Power Electron.*, vol. 19, no. 5, pp. 1205–1213, 2004.

[17] Y. A. R. I. Mohamed and E. F. El-Saadany, "Adaptive decentralized droop controller to preserve power sharing stability of paralleled inverters in distributed generation microgrids," *IEEE Trans. Power Electron.*, vol. 23, no. 6, pp. 2806–2816, 2008.

[18] P. Gupta, R. S. Bhatia, and D. K. Jain, "Active ROCOF Relay for Islanding Detection," *IEEE Trans. Power Deliv.*, vol. 32, no. 1, p. 420 429, 2017.

[19] E. Namor, F. Sossan, E. Scolari, R. Cherkaoui, and M. Paolone, "Experimental Assessment of the Prediction Performance of Dynamic Equivalent Circuit Models of Grid-connected Battery Energy Storage Systems," in *IEEE PES ISGT Europe*, 2018, no. June.

[20] U. Datta, A. Kalam, and J. Shi, "Battery Energy Storage System to Stabilize Transient Voltage and Frequency and Enhance Power Export Capability," *IEEE Trans. Power Syst.*, 2018.

[21] H. Jin, "Behavior-mode simulation of power electronic circuits," *IEEE Trans. Power Electron.*, vol. 12, no. 3, pp. 443–452, 1997.

[22] J. Peralta, H. Saad, S. Dennetière, J. Mahseredjian, and S. Nguefeu, "Detailed and averaged models for a 401-level MMC-HVDC system," *IEEE Trans. Power Deliv.*, vol. 27, no. 3, pp. 1501–1508, 2012.